Inversion of ocean surface currents to obtain coseismic seafloor deformation.

Rodrigo Cifuentes-Lobos[1], Jörn Behrens[1], Ignacia Calisto[2]
Universität Hamburg, Dept. of Mathematics, Hamburg, Germany[1]
Universidad de Concepción, Depto. de Geofísica, Concepción, Chile[2]

Universität Hamburg
DER FORSCHUNG | DER LEHRE | DER BILDUNG

This presentation participates in OSPP
EGU
Outstanding Student & PhD candidate Presentation contest
Sharing not permitted

Abstract

Introduction

- Tsunamigenic earthquakes generate sea surface current fields directly over the source.
- We relate vertical deformation with currents fields using a linear fluid model.
- We present a method for inverting dense sea surface current fields induced by tsunamigenic earthquakes to determine the distribution of deformation at the sea bottom, assuming a flat ocean floor and instantaneous deformation.

Current model

- Given an instantaneous deformation field $d(x, y)$[1]:

$$\mathbf{v_h}(x,y,t) = \frac{-i}{(2\pi)^2}\int_{-\infty}^{\infty}\int_{-\infty}^{\infty} dk_x dk_y e^{i(k_x x + k_y y)} \times \omega_0 \sin(\omega_0 t)\frac{\hat{d}(k_x,k_y)}{\sinh(kh_0)}\frac{\mathbf{k_h}}{k} \quad (1)$$

where $\hat{d}(k_x, k_y)$ is the Fourier transform of $d(x, y)$

- We discretize and take the real part

$$\widetilde{v_h}(x,y,t) = \frac{\sqrt{2g_0}}{(2\pi)^2}\sum_{i=1}^{N_x}\sum_{j=1}^{N_y}\frac{\sin(k_{x,i}x + k_{y,j}y)k_{h,i;j}}{\sqrt{k_{ij}\sinh(2k_{ij}h_0)}} \times \sin(\omega_{0,ij}t)\hat{d}(k_{x,i},k_{y,j})\Delta k_x \Delta k_y \quad (2)$$

- We get linear systems of equations for $\hat{d}(k_x, k_y)$ for both components

$$\mathbf{v} = \mathbf{G}\hat{\mathbf{d}} \quad (3)$$

Where $\mathbf{v} \in \mathbb{R}^{N_x N_y \times 1}$, $\mathbf{G} \in \mathbb{R}^{N_x N_y \times N_x N_y}$ and $\hat{\mathbf{d}} \in \mathbb{R}^{N_x N_y \times 1}$.

- We solve for $\hat{d}(k_x, k_y)$ and compute the inverse Fourier transform to get $d(x, y)$

Synthetic tests

- Checkerboard tests (Fig. 1).

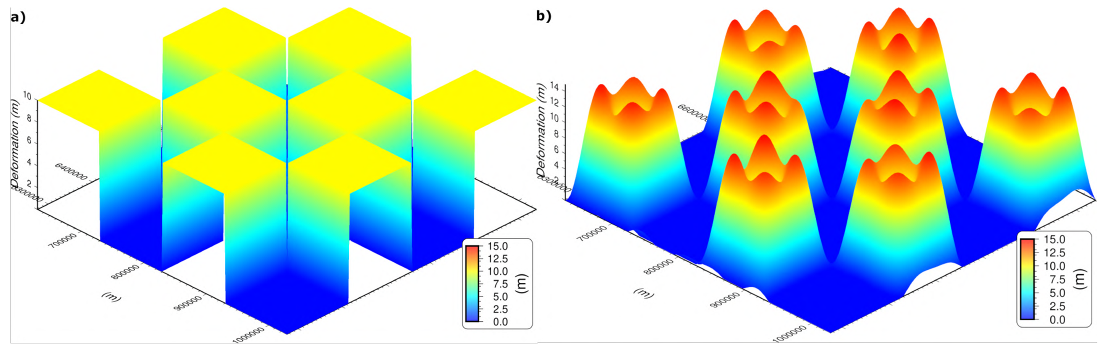

Fig 1. Input checkerboard test (left); Recovered deformation inverted 0.1 (s) after the deformation (right). Spatial resolution is constant across inversion domain.

- Gaussian bell-shaped deformation recovery with different settings and noise levels (Fig. 2).

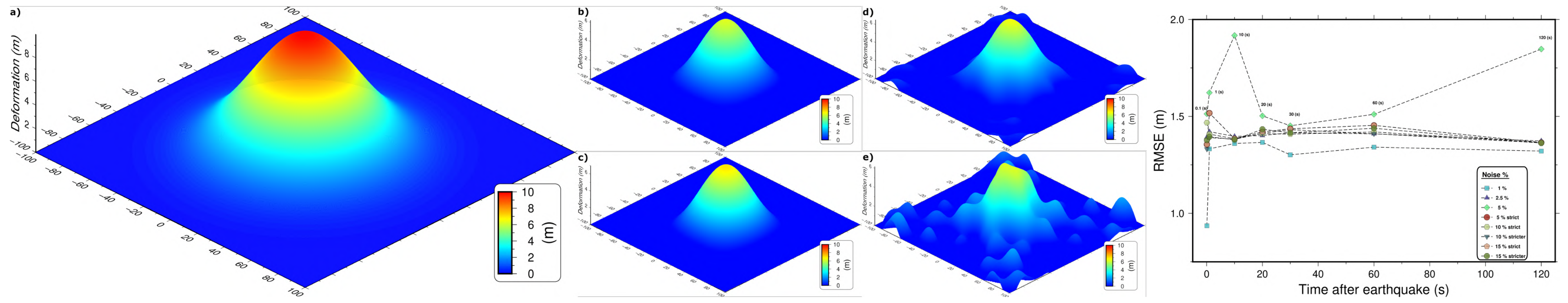

Fig 2. Gaussian bell input (a). Estimations from: Simultaneous inversion (b). Average (c). Inversion at 30 (s) with 2.5 % noise (d). Inversion at 30 (s) with 5 % noise (e) and soft constraints (left panel). RMSE of inversions with different noise levels (right panel).

Real coseismic deformations

- 8.3 Mw Illapel 2015 earthquake tests (Fig. 3).

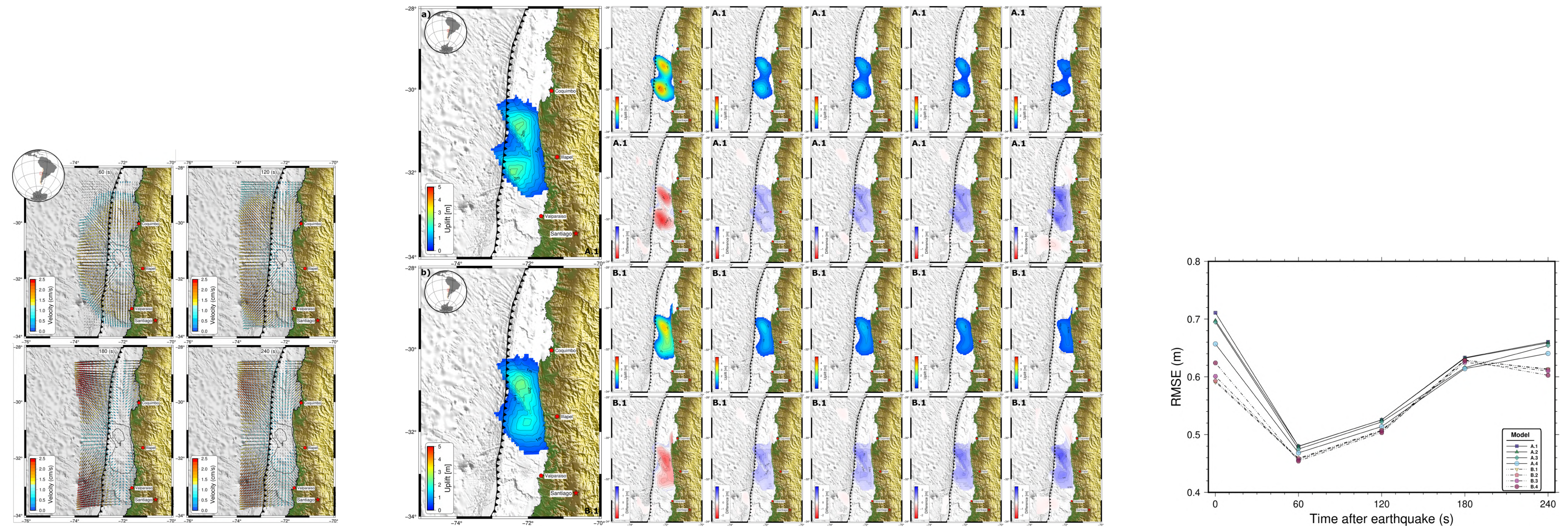

Fig 3. Current fields at 60, 120, 180 and 240 (s) after deformation (left). Inversion results of different Illapel 2015 deformation models[2,3] (center). RMSE across models (right).

- 8.8 Mw Maule 2010 earthquake test[4] (Fig. 4).

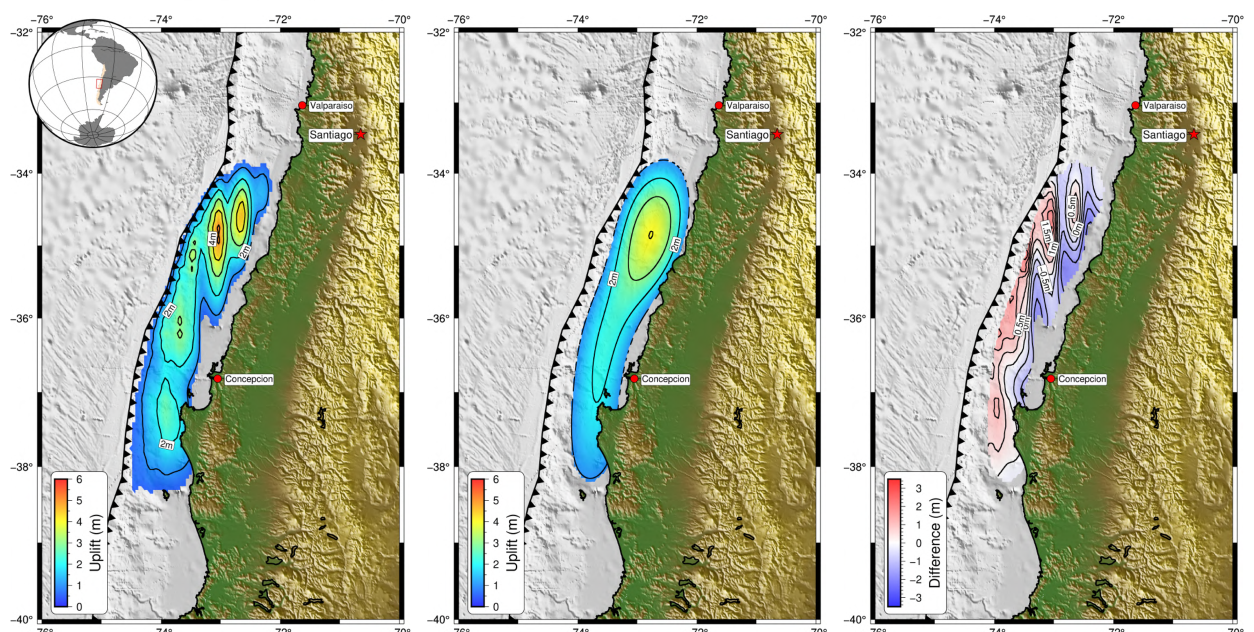

Fig 4. Maule 2010 uplift derived from slip distribution from [4] (left). Average of deformation estimations at 0.1, 1, 10, 20, 30, 60, 120, 180 and 240 (s) (center). Difference between the input deformation model and the estimated from currents (right).

Inversion scheme

- We use p linear equality constraints on $\hat{d}$ of the form

$$\mathbf{H}\hat{\mathbf{d}} = \mathbf{h} \ (4), \qquad \mathbf{H} \in \mathbb{R}^{p \times N_x N_y}, \ \ \mathbf{h} \in \mathbb{R}^{p \times 1}$$

- Rewrite (3) to account for uncertainties as

$$\mathbf{F}\hat{\mathbf{d}} = \mathbf{f} \quad (5)$$

where,

$$\mathbf{F} = \begin{bmatrix} ([\mathrm{cov}\,\mathbf{e}] + [\mathrm{cov}\,\mathbf{g}])^{\frac{-1}{2}}\mathbf{G} \\ [\mathrm{cov}\,\mathbf{h}]^{\frac{-1}{2}}\mathbf{H} \end{bmatrix}, \ \mathbf{f} = \begin{bmatrix} ([\mathrm{cov}\,\mathbf{e}] + [\mathrm{cov}\,\mathbf{g}])^{\frac{-1}{2}}\mathbf{v} \\ [\mathrm{cov}\,\mathbf{h}]^{\frac{-1}{2}}\mathbf{h} \end{bmatrix}$$

- We solve (5) with biconjugate gradient for both components and obtain the deformation with

$$\mathbf{d}^{\mathbf{est}} = \mathcal{F}\left\{\frac{\hat{\mathbf{d}}_{\mathbf{x}} + \hat{\mathbf{d}}_{\mathbf{y}}}{2}\right\}^{-1} \quad (6)$$

- We invert single time steps, multiple time steps simultaneously and average individual time steps (Fig. 2).

Conclusions

- Constant spatial resolution (Fig. 1).
- Extents and patterns are recovered.
- Only underwater portion of deformation is recovered.
- Deformation tends to be underestimated.
- High spatial frequencies are not recovered.
- Errors tend to grow as time passes.
- Origin time of the earthquake has to be known.
- Averaging individual inversions yields lower error.

References

1. Saito, T. (2013). Dynamic tsunami generation due to sea-bottom deformation: Analytical representation based on linear potential theory. *Earth, Planets and Space*, 65, 1411-1423.
2. Metois, M., Vigny, C., Socquet, A. (2016). Interseismic coupling, megathrust earthquakes and seismic swarms along the Chilean subduction zone (38â18 S). *Pure and Applied Geophysics*, 173, 1431-1449.
3. Moreno, M., Melnick, D., Rosenau, M., Bolte, J., Klotz, J., Echtler, H., ... & Oncken, O. (2011). Heterogeneous plate locking in the SouthâCentral Chile subduction zone: Building up the next great earthquake. Earth and Planetary Science Letters, 305(3-4), 413-424.
4. Moreno, M., Melnick, D., Rosenau, M., Baez, J., Klotz, J., Oncken, O., ... & Hase, H. (2012). Toward understanding tectonic control on the Mw 8.8 2010 Maule Chile earthquake. Earth and Planetary Science Letters, 321, 152-165.